Ground-state properties of ^{5}H from the ^{6}He(d,^{3}He)^{5}H reaction

A. H. Wuosmaa,[1,2,*] S. Bedoor,[1,2,†] K. W. Brown,[3,‡] W. W. Buhro,[4] Z. Chajecki,[4] R. J. Charity,[3] W. G. Lynch,[4] J. Manfredi,[4] S. T. Marley,[5,§] D. G. McNeel,[1,2] A. S. Newton,[2] D. V. Shetty,[6] R. H. Showalter,[4] L. G. Sobotka,[3] M. B. Tsang,[4] J. R. Winkelbauer,[4,‖] and R. B. Wiringa[7]

[1]*Department of Physics, University of Connecticut, Storrs, Connecticut 06268-3046, USA*
[2]*Department of Physics, Western Michigan University, Kalamazoo, Michigan 49008-5252, USA*
[3]*Departments of Chemistry and Physics, Washington University at St. Louis, St. Louis, Missouri 63130, USA*
[4]*National Superconducting Cyclotron Laboratory and Department of Physics and Astronomy, Michigan State University, East Lansing, Michigan 48824, USA*
[5]*Department of Physics and Astronomy, University of Notre Dame, South Bend, Indiana 46558, USA*
[6]*Department of Physics, Grand Valley State University, Allendale, Michigan 49401, USA*
[7]*Physics Division, Argonne National Laboratory, Argonne, Illinois 60439, USA*

(Received 3 October 2016; published 11 January 2017)

We have studied the ground state of the unbound, very neutron-rich isotope of hydrogen ^{5}H, using the ^{6}He(d,^{3}He)^{5}H reaction in inverse kinematics at a bombarding energy of $E(^6\text{He}) = 55A$ MeV. The present results suggest a ground-state resonance energy $E_R = 2.4 \pm 0.3$ MeV above the $^3\text{H} + 2n$ threshold, with an intrinsic width of $\Gamma = 5.3 \pm 0.4$ MeV in the ^{5}H system. Both the resonance energy and width are higher than those reported in some, but not all previous studies of ^{5}H. The previously unreported ^{6}He(d,t)^{5}He$_{\text{g.s.}}$ reaction is observed in the same measurement, providing a check on the understanding of the response of the apparatus. The data are compared to expectations from direct two-neutron and dineutron decay. The possibility of excited states of ^{5}H populated in this reaction is discussed using different calculations of the $^6\text{He} \rightarrow {}^5\text{H} + p$ spectroscopic overlaps from shell-model and *ab initio* nuclear-structure calculations.

DOI: 10.1103/PhysRevC.95.014310

I. INTRODUCTION

The very exotic neutron-rich isotopes of hydrogen represent the systems closest to pure neutron matter that can be produced in the laboratory. Their properties give important constraints to theories describing diffuse neutron matter, nucleon-nucleon interactions, and test a variety of different calculational methods that can be used to understand loosely bound or unbound light nuclei. The existence of pure neutron systems remains controversial. Suggestions of correlated "dineutron" emission have recently been reported [1–3]. Experimental reports supporting the observation of the tetraneutron have also appeared [4,5]. Some theoretical analyses indicate that it should not be stable or quasistable [6,7], although a recent report of no core shell model (NCSM) calculations for ^4n suggests the possibility of a broad, low-lying resonance [8]. The possibility that the exotic isotope of hydrogen ^{5}H, just one proton away from the tetraneutron, could be observable was proposed over 50 years ago (Refs. [9–11] and references therein). ^{5}H, as well as even heavier isotopes of hydrogen such as ^{6}H and ^{7}H [12–15], have been the focus of considerable recent scrutiny.

On theoretical grounds, the odd-A systems such as ^{5}H and ^{7}H should be more bound than the even-A isotopes ^{4}H and ^{6}H due to neutron pairing, perhaps making ^{5}H, or even ^{7}H long-lived enough to be observed as resonant final states in transfer reactions [7,16]. Evidence in the literature for the existence of ^{7}H is contradictory, and the most recent study [15] casts some doubt on earlier claims of its observation [12–14]. For ^{5}H the evidence is more compelling. Here we present a new study of ^{5}H with new determinations of the ground-state resonance energy and width.

An early suggestion of a possible ^{5}H ground state was reported in 1968 by Young *et al.* [17] who studied the $^3\text{H}(t,p)^5\text{H}$ reaction at a ^{3}H bombarding energy of 22.25 MeV. In that work, Young *et al.* observed a broad (1 to 2 MeV wide) feature in the proton spectra from the reaction peaked at 1.8 MeV above the $^3\text{H} + 2n$ threshold (here the resonance energies of unbound systems are expressed with respect to the threshold for decay into their constituents). Although the results were suggested to be consistent with a resonance decaying by the emission of a dineutron, the similarity of the spectra to a four-body phase space calculation suggested that more detailed measurements were necessary to make meaningful statements about ^{5}H. Since that time, a variety of somewhat contradictory experimental results on ^{5}H have been reported.

In 2001 Korsheninnikov *et al.* reported a peak in the missing-mass spectrum for the $^6\text{He}(p,2p)^5\text{H}$ reaction at $E_R = 1.7 \pm 0.3$ MeV, with a width of $\Gamma = 1.9 \pm 0.4$ MeV [18]. The bombarding energy in that case was $E(^6\text{He}) = 36A$ MeV. Golovkov *et al.*, remeasured the $^3\text{H}(t,p)^5\text{H}$ reaction at a higher bombarding energy of 57.5 MeV, reporting $E_R = 1.8$ MeV, similar to [17], but with $\Gamma \leqslant 0.5$ MeV, limited by the

*Corresponding author: alan.wuosmaa@uconn.edu
†Present address: Texas A & M University, College Station, TX 77843-4242.
‡National Superconducting Cyclotron Laboratory and Department of Physics and Astronomy, Michigan State University, E. Lansing MI, 48824, USA.
§Louisiana State University, Baton Rouge, LA 70803-4001, USA.
‖Los Alamos National Laboratory, Los Alamos, NM 87545, USA.

experimental resolution [19]. This small width conflicted with an R-matrix analysis [20] as well as with predictions from other theoretical analyses of ^{5}H (see below). Possible excited states [21], and a high-statistics correlation analysis of the $^3\mathrm{H}+2n$ decay products of ^{5}H populated in that reaction [22] have also been described. A structure corresponding to a ground-state resonance is less prominent in missing-mass spectra presented in Refs. [21,22], however, and it was suggested that the narrow structure reported in Ref. [19] may be due to interference effects from excited states. Also, it was suggested that the two-neutron transfer reaction should only weakly populate the $1/2^+$ ground state.

One-proton removal from ^{6}He has been suggested as a particularly favorable mechanism for producing ^{5}H in its ground state [7,23]. In addition to the $^6\mathrm{He}(p,2p)^5\mathrm{H}$ reaction used by Korsheninnikov, Meister *et al.* reported $^3\mathrm{H}+2n$ correlations from proton-knockout data from ^{6}He on a ^{12}C target [24], and gave a resonance energy $E_R = 2.5$–3.0 MeV and width $\Gamma = 3$–4 MeV, rather different from earlier results. Another proton-removal reaction that could be used to search for ^{5}H is $^6\mathrm{He}(d,^3\mathrm{He})^5\mathrm{H}$. Some reports of this reaction [25–27] exist. Reference [25] gives a very narrow ground-state resonance at $E_R = 1.8$ MeV, similar to that given in Ref. [19]. Other data for the same reaction obtained under similar conditions [26,27] suggest higher resonance energies and larger widths. Indications of highly excited proton-decaying states in ^{5}He were also made from $^3\mathrm{H}+p+n$ coincidence events, although the neutron-unbound ground state in ^{5}He could not be observed due to the experimental conditions.

Finally, reports of the ^{5}H ground state have also been made from pion absorption [28,29]. The resonance energies and widths from pion reactions are substantially larger ($E_R \approx 5$ MeV and $\Gamma \approx 5$ MeV) than those obtained from nucleon-transfer. The experimental situation regarding ^{5}H was reviewed in 2004 by Grigorenko [30], and previous experimental data and experimental conditions for the measurements are summarized in Table I.

The theoretical situation regarding ^{5}H is also complex. Should it exist, ^{5}H would possess a ground-state spin and parity of $J^\pi = 1/2^+$. Most theoretical treatments also contain predictions for $3/2^+$ and $5/2^+$ excited states. Many studies of ^{5}H have utilized cluster-models of the three-body ^{3}H-n-n system [31–34], often employing hyperspherical-harmonics expansions [7,23,34–36]. A number of these calculations have been performed with interactions determined using existing nucleon-scattering phase-shift data [36]. Predictions for the resonance energy and width vary considerably. These typically range from E_R near 1 MeV to as high as 3 MeV, and widths from as narrow as 0.6 MeV [34] to as large as 4 MeV [7,32], with most values clustering around $E_R \approx 1.5$ to 2.0 MeV, and $\Gamma \approx 1$ to 2 MeV. Finally, it is also interesting to note that ^{5}H is important in the context of the hypernucleus $^6_\Lambda$H, which has recently been suggested to exist as a particle-bound system [37]. The calculations of Gal and Millener [38], and Himaya *et al.* [39], tie the binding energy of $^6_\Lambda$H to the resonance energy of ^{5}H. Table II lists some references for theoretical works on ^{5}H, with the predictions for the energy and width of the ^{5}H ground state. Although many of these results also discuss excited states in this paper we focus on the ^{5}H ground state and list only predictions for that level.

Here we present the results of a new experimental study of the $^6\mathrm{He}(d,^3\mathrm{He})^5\mathrm{H}_{\mathrm{g.s.}}$ reaction. The most notable difference between this experiment and previous works is the bombarding energy which is significantly higher than the values used in earlier studies of this reaction. Due to the extremely negative ground-state Q value, expected to be near -20 MeV, depending on the mass of ^{5}H, energy conservation and momentum matching can restrict the range of accessible excitation energy in ^{5}H, distorting the experimental lineshape and affecting the deduced energy and width of ^{5}H resonances. Such an effect has been discussed in Ref. [22] in the context of the $^3\mathrm{H}(t,p)^5\mathrm{H}$ reaction and we discuss in detail the implications of such effects in the $^6\mathrm{He}(d,^3\mathrm{He})^5\mathrm{H}_{\mathrm{g.s.}}$ reaction. Here, both the $^6\mathrm{He}(d,^3\mathrm{He})^5\mathrm{H}_{\mathrm{g.s.}}$ and the previously unreported $^6\mathrm{He}(d,t)^5\mathrm{He}_{\mathrm{g.s.}}$ reactions were observed simultaneously. The properties of the ^{5}He ground-state resonance are well known from neutron scattering and neutron-transfer reactions [40]. A side-by-side comparison of the ^{5}H results with those for $^5\mathrm{He}_{\mathrm{g.s.}}$ serves as confirmation of the method and provides additional information about the calibration and response of the apparatus.

In this paper, we first present the experimental details, followed by a discussion of the data reduction. We then discuss the ^{5}H lineshape incorporating the effects of energy conservation and momentum matching with a distorted-wave

TABLE I. Summary of experimental results for ^{5}H. Resonance energies are given relative to $^3\mathrm{H}+2n$.

Reference	Reaction	Detected	E_R (MeV)	Γ (MeV)	E_{beam} (A MeV)
[17]	$^3\mathrm{H}(t,p)^5\mathrm{H}$	p	≈ 1.8	≈ 1.5	7.42
[18]	$^6\mathrm{He}(p,2p)^5\mathrm{H}$	$2p$	1.7 ± 0.3	1.9 ± 0.4	36
[19]	$^3\mathrm{H}(t,p)^5\mathrm{H}$	t,p,n	1.8 ± 0.1	< 0.5	19.2
[21]	$^3\mathrm{H}(t,p)^5\mathrm{H}$	t,p,n	≈ 2	–	19.2
[22]	$^3\mathrm{H}(t,p)^5\mathrm{H}$	t,p,n	≈ 2	≈ 1.3	19.2
[24]	$^6\mathrm{He}(^{12}\mathrm{C},X+2n)^5\mathrm{H}$	$t,2n$	≈ 3	≈ 6	240
[25]	$^6\mathrm{He}(d,^3\mathrm{He})^5\mathrm{H}$	^{3}He ,t	1.8 ± 0.1	< 0.6	22
[26]	$^6\mathrm{He}(d,^3\mathrm{He})^5\mathrm{H}$	^{3}He ,t	1.8 ± 0.2	1.3 ± 0.5	22
[27]	$^6\mathrm{He}(d,^3\mathrm{He})^5\mathrm{H}$	^{3}He ,t	1.7 ± 0.3	≈ 2.5	22
[28]	$^9\mathrm{Be}(\pi^-,pt)^5\mathrm{H}$	p,t	5.2 ± 0.3	5.5±0.5	$E_\pi < 30$ MeV
[28]	$^9\mathrm{Be}(\pi^-,dd)^5\mathrm{H}$	p,t	6.1 ± 0.4	4.5±1.2	$E_\pi < 30$ MeV

TABLE II. Summary of some theoretical results for ^{5}H. Resonance energies are given relative to $^3\mathrm{H} + 2n$.

Reference	Method	E_R (MeV)	Γ (MeV)
[7]	Cluster, model with source	2–3	4–6
[23]	Three-body cluster	2.5–3	3–4
[31,35]	Cluster, J-matrix, resonating group model	1.39	1.60
[36]	Cluster, complex scaling adiabatic expansion	1.57	1.53
[32]	Cluster, generator coordinate method	$\approx$3	$\approx$1–4
[33]	Cluster, complex scaling	1.59	2.48
[34]	Cluster, analytic coupling in continuum constant	1.9 ± 0.2	0.6 ± 0.2

Born approximation (DWBA) analysis of the reaction. Finally, we consider our results in the context of two different calculations of the $^6\mathrm{He} \rightarrow {}^5\mathrm{H} + p$ spectroscopic overlap, and attempt to reconcile some of the available experimental results.

II. EXPERIMENT

The experiment was conducted at the National Superconducting Cyclotron Laboratory (NSCL) at Michigan State University. A 55A MeV ^{6}He beam was obtained from the fragmentation of a primary 120A MeV beam of ^{18}O on a thick ^{9}Be production target. The ^{6}He fragments were isolated using the A1900 fragment separator at the NSCL. The beam intensity was approximately 7×10^5 particles per second on target as determined from the count rate observed on a scintillator detector at the focal plane of the A1900, and an estimated transport efficiency of 80% consistent with previous observations. The momentum spread, determined by slits at the exit of the A1900 separator, was 1%. The ^{6}He beam was greater than 95% pure, containing a $< 5\%$ ^{8}Li impurity with an energy of approximately 315 MeV. Reactions from the ^{8}Li contaminant were eliminated using the event selections described below. The size of the beam spot on the target was approximately 10 mm wide horizontally with a 5–6 mm vertical width. The contributions to the experimental resolution from the beam-spot size are discussed below. The ^{6}He beam bombarded thin targets consisting of 1.9 mg/cm^2 $(\mathrm{CD}_2)_n$ and 1.2 mg/cm^2 ^{12}C foils; the ^{12}C target was used to assess the backgrounds from the ^{12}C present in the $(\mathrm{CD}_2)_n$ target. The thickness of the $(\mathrm{CD}_2)_n$ target was determined using α-transmission measurements as well as by direct weighing of the $(\mathrm{CD}_2)_n$ material, and is reliable to 10%.

The reaction products were detected and identified using the High Resolution Array (HiRA) [41]. HiRA is an array of charged-particle-detector telescopes, with particle identification provided by segmented silicon detectors and CsI(Tl) scintillator crystals. For this experiment, HiRA consisted of 14 telescopes covering laboratory angles between 2 and 14 degrees, corresponding to angles in the center-of-mass system ranging from about 1 to 10 degrees. The solid-angle coverage of HiRA is identical to that described in Ref. [42].

Although the beam energy is high, in the inverse-kinematic $(d,{}^3\mathrm{He})$ and (d,t) reactions the ^{3}He and ^{3}H reaction products have small kinetic energies. These kinetic energies are between 10 and 12 MeV for ^{3}He, and near 5 MeV for ^{3}H, at laboratory angles that correspond to the situation where the ^{3}He or ^{3}H particles are emitted to forward center-of-mass angles in normal kinematics. These angles are where the reaction yields are expected to be the greatest.

The energies of the ^{3}H or ^{4}He produced from $^5\mathrm{H} \rightarrow {}^3\mathrm{H} + 2n$ or $^5\mathrm{He} \rightarrow {}^4\mathrm{He} + n$ decays are far higher, between 140 and 300 MeV. To contend with this wide dynamic range, HiRA was configured with two silicon-detector (Si) layers with thicknesses of 65 and 1500 μm, respectively, backed by four four-cm thick CsI(Tl) crystals. The first Si layer [the ΔE(Si) detector] was divided into 32 2-mm wide strips. The second layer [the E(Si) detector] was a double-sided strip detector (DSSD) with 32 horizontal and 32 vertical strips, also each 2 mm wide. Each DSSD pixel subtended 0.13 degrees in the laboratory. The low-energy particles stopped in the second Si layer, and were identified by energy loss in the two Si detectors. The more energetic particles penetrated both Si layers, typically depositing between 3–10 MeV for ^{3}H and 10–15 MeV for ^{4}He in those detectors. These higher-energy particles were identified by energy loss in the second Si layer and the CsI(Tl) crystals. For some ^{3}H particles, the kinetic energy was large enough (greater than approximately 187 MeV) that they could penetrate both the Si and CsI(Tl) detectors, although all ^{4}He particles of interest were fully stopped. These "punch-through" ^{3}H ions had a different particle-identification signature than those that stopped in the CsI(Tl) crystals and were rejected from the analysis. The influence of this effect was studied using Monte Carlo simulations and is discussed below.

The decay neutrons were not detected in this measurement. The coincident detection of the low-energy reaction and high-energy decay products in different HiRA telescopes provided a clean signature for the transitions of interest. The Si detectors were calibrated using α particles from a radioactive ^{228}Th source, with a typical intrinsic Si-detector energy resolution of 50 keV. Calibration of the CsI(Tl) crystals was accomplished using the scattered ^{6}He beam, as well as a beam consisting primarily of 168 MeV ^{3}H that was scattered from the ^{12}C target.

Figures 1 and 2 show particle-identification (PID) spectra from the Si-CsI(Tl) and Si-Si telescopes, for the $^6\mathrm{He}(d,{}^3\mathrm{He})^5\mathrm{H}$ and $^6\mathrm{He}(d,t)^5\mathrm{He}$ reactions, respectively. In each figure, panels (a) and (c) show data from the Si-CsI(Tl) detectors that identify high-energy particles observed in coincidence with the corresponding low-energy particle identified in the two Si-detector layers. Panels (b) and (d) show data from the two Si-detector layers for events where the corresponding high-energy particle of interest was identified using the Si-CsI(Tl) detectors. Also in each figure, panels (a) and (b) represent

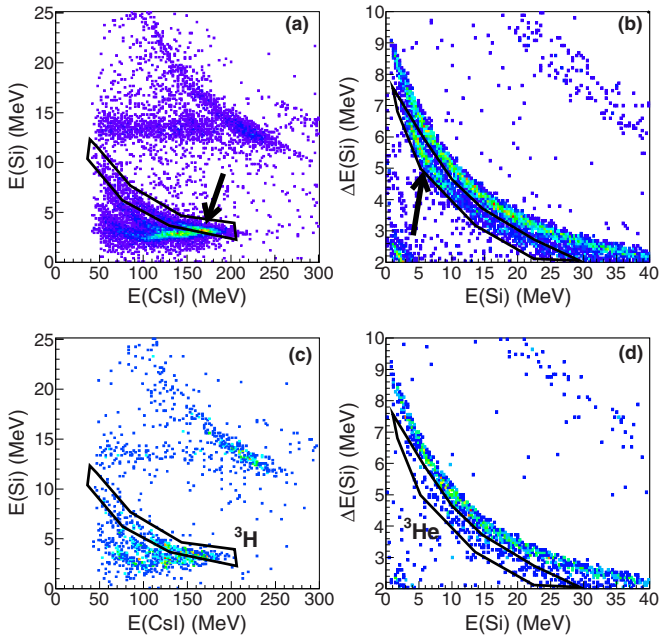

FIG. 1. PID spectra for the ^{6}He(d,^{3}He)^{5}H reaction. (a) and (c) ^{3}H particle-identification spectra from the Si-CsI(Tl) telescopes, for events with a low-energy ^{3}He particle identified in the Si-Si telescopes. (a) $(CD_2)_n$ target, (c) ^{12}C target. The polygons correspond to identified ^{3}H particles, and the arrow in (a) points to the location expected for the ^{3}H particles of interest. (b) and (d): ^{3}He PID spectra from the Si-Si telescopes, for events with a high-energy ^{3}H particle identified in the Si-CsI(Tl) telescopes. (b) $(CD_2)_n$ target, (d) ^{12}C target. The polygons correspond to identified ^{3}He particles, and the arrow in (b) points to the location expected for the ^{3}He particles of interest. The ^{3}He enhancement for the $(CD_2)_n$ target is absent with the ^{12}C target.

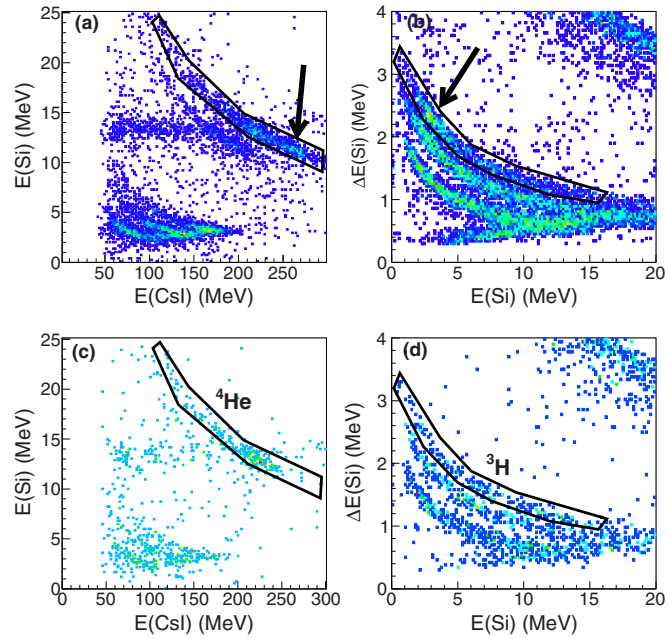

FIG. 2. PID spectra for the ^{6}He(d,t)^{5}He reaction. (a) and (c) ^{4}He particle-identification spectra from the Si-CsI(Tl) telescopes, for events with a low-energy ^{3}H particle identified in the Si-Si telescopes. (a) $(CD_2)_n$ target, (c) ^{12}C target. The polygons correspond to identified ^{4}He particles, and the arrow in (a) points to the location expected for the ^{4}He particles of interest. (b) and (d) ^{3}H PID spectra from the Si-Si telescopes, for events with a high-energy ^{4}He particle identified in the Si-CsI(Tl) telescopes. (b) $(CD_2)_n$ target, (d) ^{12}C target. The polygons correspond to identified ^{3}H particles, and the arrow in (b) points to the location expected for the ^{3}H particles of interest. The ^{3}H enhancement for the $(CD_2)_n$ target is absent with the ^{12}C target.

data obtained with the $(CD_2)_n$ target, and panels (c) and (d) show the data obtained with the ^{12}C target. In the figures for each reaction, the arrows in panels (a) and (b) point to regions of enhanced yield where the products of the ^{2}H induced reactions are expected and observed. While some low-energy ^{3}He or ^{3}H particles are observed with the ^{12}C target, the enhancements in the yields of these particles in the interesting regions disappear. For the high-energy particles, for all data we observe a strong group near E(CsI) $\approx$ 220 MeV, E(Si) $\approx$ 13 MeV that corresponds to ^{4}He nuclei produced by direct fragmentation of the ^{6}He beam.

III. DATA REDUCTION

The kinetic energies of the low-energy particles were obtained from the sum of the signals obtained from the two Si layers. Figures 3(a) and 3(b) show kinetic-energy spectra for the low-energy ^{3}He and ^{3}H reaction products, for all laboratory angles. The data are selected by requiring a coincidence with either a high-energy ^{3}H or ^{4}He particle for panels (a) and (b), respectively. The kinetic-energy spectra are not corrected for energy loss in the target; assuming that the reaction takes place in the center of the target, a 10 MeV ^{3}He particle loses approximately 480 keV, while a 5 MeV ^{3}H loses approximately 200 keV in the $(CD_2)_n$ with energy losses calculated according to the method described in [46] used in the codes SRIM [47] and LISE++ [48]. The peaks near $E(^3\text{He}) = 10$ MeV and $E(^3\text{H}) = 5$ MeV correspond to the ground states of ^{5}H and ^{5}He, respectively. The filled histogram in Fig. 3(a) represents data collected with the ^{12}C target, and is scaled to the $(CD_2)_n$ target data according to the number of beam particles detected in the focal-plane scintillator of the A1900 separator and the known target thicknesses. The ^{12}C target data show no evidence of a peak at any energy. For low-energy ^{3}H, no events survive the event-selection criteria for the ^{12}C target.

Additional information about the reaction can be obtained by studying the correlation between the kinetic energies of the low- and high-energy particles. Figures 4(a) and 4(b) show the recoil energy plotted versus kinetic energy of the low-energy particle for (a) ^{3}He-^{3}H coincidences from the ^{6}He(d,^{3}He)^{5}H reaction or (b) ^{3}H-^{4}He coincidences from the ^{6}He(d,t)^{5}He reaction. Figures 4(c) and 4(d) show the results of Monte Carlo simulations of this correlation for the (d,^{3}He) and (d,t) reactions, respectively. Details of the Monte Carlo simulations are given below. The horizontal dashed lines indicate the recoil energies accepted for further analysis of the data. This event selection has little effect except in the case of alpha particles in Fig. 4(b), where the restriction is necessary to suppress events arising from $^6\text{He} \rightarrow {}^4\text{He} + 2n$ breakup.

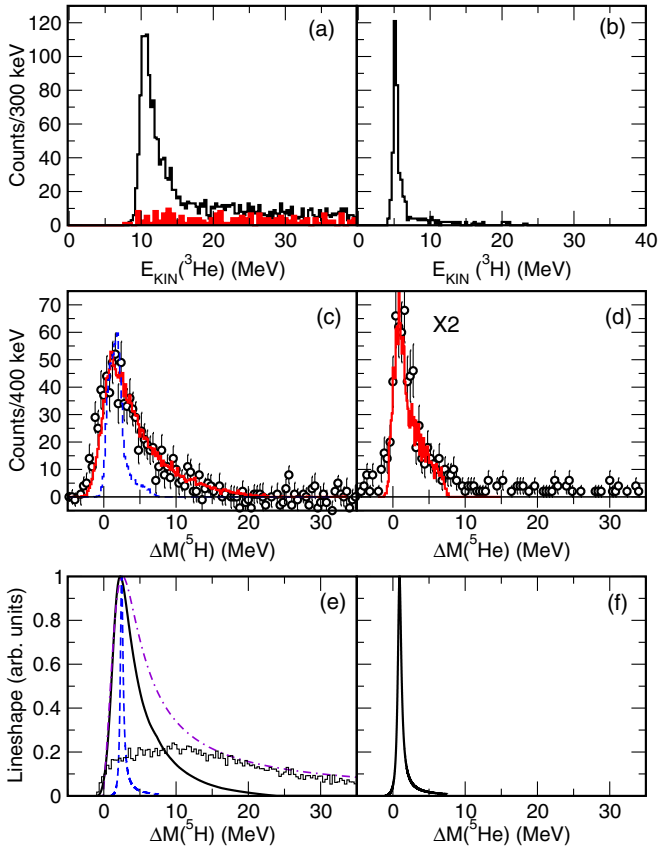

FIG. 3. (a),(b) Kinetic-energy spectra of low-energy ^{3}He and ^{3}H particles measured in the Si-detector telescopes. The filled histogram in (a) shows the background from the measurement with the ^{12}C target. (c),(d) ^{5}H and ^{5}He missing-mass spectra. The solid histograms in (c) and (d) and dashed histogram in (c) correspond to the simulated experimental lineshapes obtained by filtering the lineshape-curves shown in (e) and (f) through the response of the apparatus. In (e), the dot-dashed and solid curves represent the intrinsic and DWBA-modified lineshapes that produce a best fit to the data in (c), and the dashed curve is a narrow lineshape identical to that shown in (f). (f) Intrinsic lineshape for ^{5}He calculated with from parameters given in the literature. The ^{3}He -^{3}H coincidence efficiency for the ^{5}H measurement appears as the histogram in (e) with the vertical scale the same as that of the left axis.

The ^{5}H or ^{5}He mass is calculated as $m_5 = \sqrt{(E_0 - E_3)^2 - p_1^2 - p_3^2 + 2p_1p_3\cos\theta_3}$, where $E_0 = T_{\rm beam} + m_{\rm beam} + m_{\rm target}$, T is the kinetic energy, E_3, p_3, and θ_3 are the total energy, momentum, and laboratory angle of the mass-3 particle, and p_1 is the momentum of the beam, in units where $c = 1$. The data points in Figs. 3(c) and 3(d) show the ^{5}H and ^{5}He mass spectra, plotted relative to the ^{3}H + 2n or ^{4}He + n thresholds, respectively. In the case of ^{5}H, the data are background-subtracted using the data obtained with the ^{12}C target; similar to the background in the ^{3}He kinetic-energy spectrum, this background is featureless throughout the experimental missing-mass range. As with the kinetic-energy spectra, the missing-mass spectra are not corrected here for energy loss in the target. The missing-mass

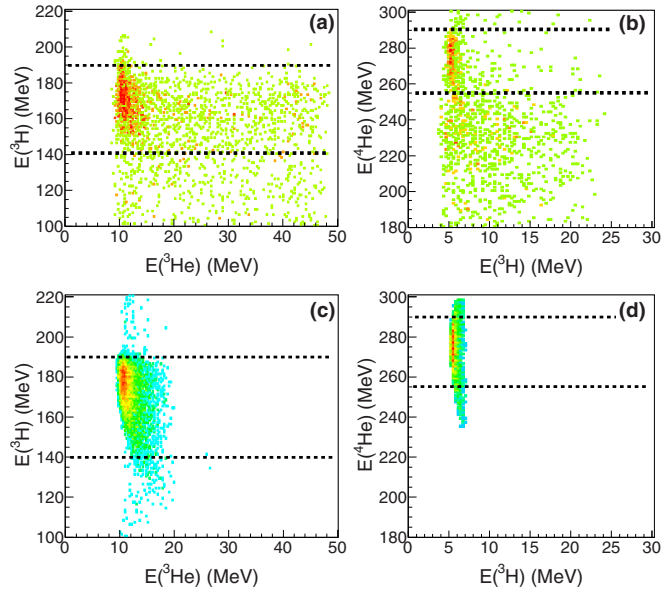

FIG. 4. Correlation between (a) $E(^3\text{He})$ and $E(^3\text{H})$ and (b) $E(^3\text{H})$ and $E(^4\text{He})$ from the ^{6}He(d,^{3}He)^{5}H and ^{6}He(d,t)^{5}He reactions, respectively. (c),(d) Energy correlations obtained from Monte Carlo simulations described in the text. Good events are selected from the regions between the dashed lines. The z axes are logarithmic.

dependence of the ^{3}He -^{3}H coincidence efficiency for the ^{5}H measurement appears as the histogram in Fig. 3(e). For ^{5}H, the data reveal a broad peak with a maximum near 1.8 MeV and an experimental width of approximately 5.5 MeV. As is the case with the kinetic energy, the peak in the ^{5}He missing-mass spectrum is much narrower, with a maximum near 0.8 MeV and width of approximately 1.5 MeV FWHM. The histograms in Figs. 3(c) and 3(d) represent fits to the data using a Monte Carlo procedure and are described below, as are the lineshapes that appear in Figs. 3(e) and 3(f).

IV. PEAK FITTING AND LINESHAPE ANALYSIS

A Monte Carlo peak-fitting approach was used to estimate the resonance energy and width for ^{5}H. This process starts by assuming different resonance profiles for the ^{5}H ground state, and here we assume that only the ground state is populated in the ^{6}He(d,^{3}He)^{5}H reaction. Nuclear-structure calculations supporting this assumption are described below. For fitting purposes only, we adopt an R-matrix prescription [49] to parametrize the initial ^{5}H line shape. We use the term "intrinsic" to describe this profile because, as discussed below, it is not the profile expected to be reflected by the data. The profile used here is given by

$$\sigma(E) \propto \frac{\Gamma}{(E - E_R)^2 + \Gamma^2/4}, \qquad (1)$$

where $\Gamma = 2P_L(E)\gamma^2$, $P_L(E)$ is the penetrability, and γ^2 is the reduced width, given by $\gamma^2 = S\gamma^2_{\rm s.p.}$. The single-particle reduced width $\gamma^2_{\rm s.p.}$ is given by $\gamma^2_{\rm s.p.} = \hbar^2/2\mu R^2$, and S is a spectroscopic factor. The radius parameter is chosen as $r_0 = 1.4$ fm. We omit the shift term as it is negligibly small here. In

calculating the ^{5}H profile we consider only the dineutron+^{3}H case as the ^{4}H core is broad and the $n + {}^4$H separation energy not well defined. We emphasize that the quantities S, $\gamma^2_{\text{s.p.}}$, and E_R are used simply as variable parameters that can be adjusted in a well-defined fashion to produce different lineshape profiles. For ^{5}He, we used the well-established values for the resonance energy and width from [40].

We used two extreme physical assumptions for the subsequent two-neutron decay: (1) that ^{5}H decay is purely "direct" or "democratic" emission of two neutrons, or (2) that ^{5}H decay is a two-body process consisting of the emission of a single dineutron. While neither of these scenarios is likely to be exactly correct, the two assumptions can test the sensitivity of the experiment to different possible neutron correlations in ^{5}H. For direct three-body decay, we assume no n-n correlation, and the two neutrons are emitted isotropically in the ^{5}H system with their energies determined solely from the ^{3}H-2n phase-space distribution, with their total available energy given by the energy of the ^{5}H system relative to $^3\text{H} + 2n$. For dineutron decay, the dineutron state is fixed according to the parameters described in Refs. [43–45], and the dineutron is emitted isotropically in the ^{5}H center-of-mass system. These choices affect only the kinetic-energy distribution of the detected ^{3}H particle.

A. Q-value dependence

An important consideration for reactions with very negative Q values that are poorly momentum matched is that the yield can depend strongly on the excitation energy of the product nucleus. For ^{6}He(d,^{3}He)^{5}H the Q value is near -15 to -20 MeV, depending on the actual resonance energy of the ^{5}H ground state. This negative Q-value limits the excitation energy attainable in the reaction through energy conservation, and in addition the Q-value dependence of the cross section can distort the profile reflected in the measured excitation-energy spectrum, especially for broad structures. Figure 5(a) shows the results of distorted-wave Born approximation (DWBA) calculations of the Q-value dependence for $\ell = 0$ proton-removal cross section with the ^{6}He(d,^{3}He)^{5}H reaction. The curves represent this dependence for bombarding energies of 55A MeV (solid curve) and 22A MeV (dashed curve) averaged between $\theta_{\text{c.m.}} = 0^\circ$ to 10°. The dot-dashed curve represents the Q-value dependence averaged between $\theta_{\text{c.m.}} = 20^\circ$ to 40° at 22A MeV. Each curve is normalized to the cross section at $Q = -12$ MeV. The calculations were performed using the code PTOLEMY [50] with optical-model parameters taken from global analyses described in Refs. [51,52], and the (d,^{3}He) vertex obtained from quantum Monte Carlo techniques as described by Brida *et al.* [53]. The calculated cross section drops significantly as the Q value becomes more negative, more strongly so for the lower bombarding energy. At very forward angles the falloff with increasingly negative Q value is monotonic, however at larger angles, due to the varying position of the first diffraction minimum in the angular distribution, the suppression can be more complicated. At more backward angles the precise Q-value dependence may be more sensitive to optical-model parameters, but should behave in a qualitatively similar way for different parameter sets.

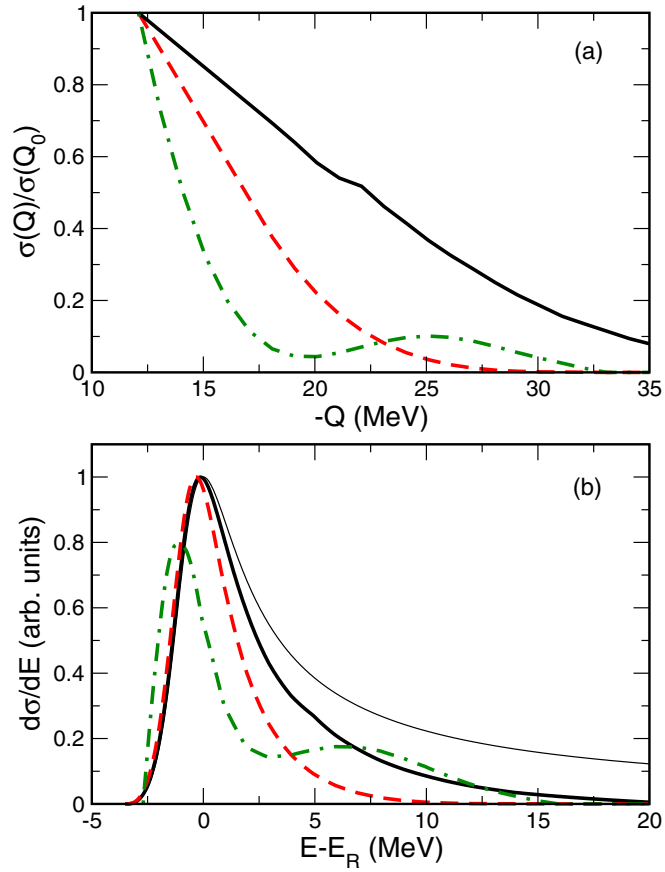

FIG. 5. (a) Q-value dependence of the ^{6}He(d,^{3}He)^{5}H cross section from DWBA calculations. The curves represent the ratio of the cross section averaged between $\theta_{\text{c.m.}} = 0^\circ$–$10^\circ$, calculated at Q MeV to that at $Q_0 = -12.5$ MeV for bombarding energies of 55A MeV (solid curve) and 22A MeV (dashed curve), and $\theta_{\text{c.m.}} = 20^\circ$–$40^\circ$ at 22A MeV (dot-dashed curve). (b) Example of the effects of Q-value dependence on the intrinsic lineshape for a state in ^{5}H. Thin solid curve: "intrinsic" profile, Thick solid curve: "laboratory" profile modified using DWBA calculations for $E_{\text{beam}} = 55A$ MeV at forward angles, dashed curve: modified profile at $E_{\text{beam}} = 22A$ MeV at forward angles, dot-dashed curve: modified for $E_{\text{beam}} = 22A$ MeV for $\theta_{\text{c.m.}} = 20^\circ$–$40^\circ$. The dot-dashed curve in (b) is multiplied by a factor of 5 for comparison with the other curves.

Figure 5(b) shows the effect of this Q-value suppression on the measurable line shape of a typical resonance in ^{5}H. The thin solid curve represents a state with a FWHM of approximately 6.3 MeV in the ^{5}H system. Widths for broad resonant states are variously defined; choosing the definition $\Gamma = 2\gamma^2 P_L(E_R)$ gives an intrinsic value of $\Gamma(E_R) = 5.3$ MeV for this lineshape. The thick solid curve illustrates this intrinsic profile modified by the forward-angle Q-value dependence at a bombarding energy of 55A MeV; we refer to this shape as the "laboratory" lineshape, which would be observed in a perfect experiment with no modification by the experimental response. The laboratory FWHM is decreased to approximately 75% of its intrinsic value. At a bombarding energy of 22A MeV (dot-dashed curve) the effect is greater with the laboratory FWHM only 55% of that of the intrinsic shape, with the laboratory peak

energy shifted approximately 350 keV lower compared to the intrinsic value. For data obtained at more backward angles, an even more complicated dependence can occur, introducing structure not present in the intrinsic resonance profile (see dot-dashed curve). In the current analysis, this suppression is applied to all intrinsic lineshapes before they are used as input to the Monte Carlo simulations described below. Due to effects such as these, care should be exercised in the interpretation of data where, due to low bombarding energies, the reaction mechanism can influence the excitation-energy profile.

B. Monte Carlo simulations

For each intrinsic profile considered, after modifying the shape using DWBA calculations, events are generated according to reaction kinematics and the chosen decay mode. The particle energies and angles are then processed through a simulation of the HiRA detector, including the effects of beam-spot size, energy loss in the target, detector resolutions consistent with those measured with sources and well-defined beams, and the incomplete stopping of energetic ^{3}H particles discussed above. The simulated experimental missing-mass spectrum is then obtained from the simulated experimental kinetic energies and scattering angles of the low-energy mass-3 particles. We refer to the final result of this process as the "experimental" lineshape that can be compared directly to the measured spectrum. We investigated the effects of target thickness and beam-spot size in these calculations. Energy loss in the target was calculated as described in [46] as implemented in the codes SRIM and LISE++; the two codes use the same stopping formalism and give essentially identical results. We also studied the effects of the extended beam spot by simulating a very narrow resonance, and comparing the resulting experimental missing-mass spectra obtained with a narrow (1 mm × 1 mm) or broad (10 mm × 10 mm) spots. Although changes in the position of the interaction in the target can modify the scattering angle, the very weak dependence of the kinetic energies of the low-energy reaction product on angle in inverse kinematics makes the resulting calculated missing mass insensitive to the spot size, and the simulated results for the narrow and broad beam spots were identical.

C. Fit results

A large number of possible intrinsic line shapes were considered and processed through the simulation chain. χ-square values were then calculated from the experimental simulated and measured missing-mass spectra. We studied the variations in χ-square as a function of resonance energy and width, determining which intrinsic line shape best reproduced the data. Figure 6 shows the dependence of chi square on the laboratory peak position (a) and width (b). Here the total number of degrees of freedom is 45. For the peak position, Fig. 6(a) the points include only intrinsic lineshapes where the "experimental" Monte Carlo FWHM agrees with that of the measured data. For the width, Fig. 6(b) includes only intrinsic lineshapes where the simulated "experimental" peak position coincides with the peak in the data. The best-fit laboratory values are $E_R = 2.4 \pm 0.3$ MeV and $\Gamma = 4.8 \pm 0.4$ MeV,

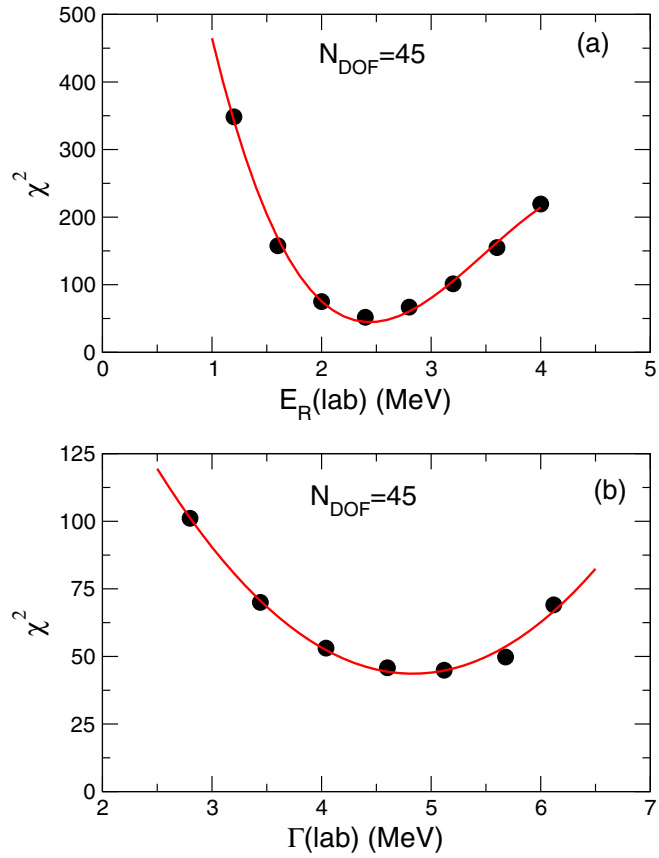

FIG. 6. Dependence of χ^2 on (a) laboratory resonance peak position, with the laboratory width held constant at its best-fit value. (b) laboratory resonance width, with the laboratory peak position held constant at its best-fit value. The lines in (a) and (b) represent polynomial fits to the χ^2 distributions of order 3 for (a) and 2 for (b), which are used to determine the final best-fit values and uncertainties. The minimum $\chi^2 = 43.6$ with 45 degrees of freedom, giving $\chi^2_\nu = 0.97$.

respectively, corresponding to an intrinsic resonance energy of $E_R = 2.4 \pm 0.3$ MeV and width $\Gamma(E_R) = 5.3 \pm 0.4$ MeV as defined above. The uncertainties include the fitting uncertainties given by the shapes of the χ-square curves of $\Delta E_R = 0.1$ MeV and $\Delta\Gamma = 0.3$ MeV, with an additional contribution from the uncertainty of the target thickness.

For comparison, the same procedure was used to generate a simulated experimental lineshape for the ^{5}He ground state, using the known values of $E_R = 0.798$ MeV and $\Gamma = 0.648$ MeV [40] [see Fig. 3(f)]. The histogram in Fig. 3(d) shows the resulting peak for this narrow state, which agrees well with the data, suggesting that the understanding of the instrumental response of the experiment and treatment of the data are reliable. The experimental missing-mass resolution determined for ^{5}H from the Monte Carlo simulations is approximately 1.8 MeV FWHM, dominated by energy loss of the low-energy ^{3}He in the target. Due to the smaller energy loss for the low-energy ^{3}H, the resolution is somewhat better, ≈1.5 MeV FWHM for the ^{5}He case.

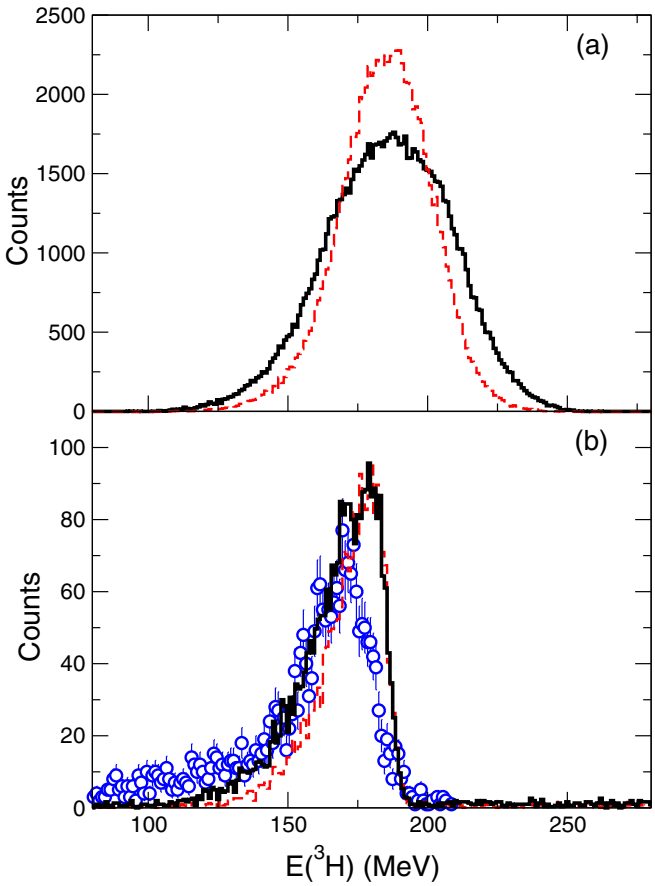

FIG. 7. ^{3}H recoil-energy distributions from the decay of ^{5}H. (a) Simulated spectra assuming "democratic" ^{5}H two-neutron decay (dashed histogram) and dineutron decay (solid histogram) before filtering through the experimental response. (b) Same as (a) but after filtering the experimental response. The points in (b) represent the experimental data, and the histograms in (b) are arbitrarily scaled to the data for purposes of comparison.

D. Beam-like recoils and two-neutron correlations

With the best-fit ^{5}H lineshape determined, we consider whether it is possible to obtain more information about the decay of this system from the distribution of ^{3}H recoil energies. The correlation between the ^{3}He and ^{3}H kinetic energies from the best-fit simulation assuming direct three-body decay appears in Fig. 4(c). The simulated distribution is very similar to the data, as is also the case for the corresponding ^{5}He calculation shown in Fig. 4(d).

To compare the expected ^{3}H kinetic-energy distributions for direct versus dineutron decays, Fig. 7(a) shows the simulated distributions from kinematics only, without including the response of the experiment. Here we used the ^{5}H resonance profile that best reproduced the data, and the solid and dashed histograms represent the direct- and dineutron-decay scenarios, respectively. The ^{3}H kinetic-energy distribution is somewhat wider in the case of dineutron emission, due to the larger "kick" received by the ^{3}H from the emitted dineutron in the ^{5}H center of mass frame compared to the two smaller "kicks" from individual uncorrelated neutrons. Figure 7(b) shows the same simulated distributions filtered through the response of the apparatus, and the corresponding data from identified ^{5}H events. The ^{3}H punch-through effect cuts off the recoil-energy distributions near 185–190 MeV, however the difference between the two decay modes is still apparent at the low-energy side of the distribution. The points in Fig. 7(b) represent the measured data. Between $E(^3\mathrm{H}) = 175$ and 200 MeV, the difference between data and simulation arises from the event selection applied to the data to identify ^{3}H; the precise shape of this selection cannot be applied directly to the simulated data. Below 175 MeV, the data suggest a slight preference for the dineutron-decay scenario. An experiment with more complete ^{3}H acceptance or additional detection of the two neutrons could provide more information about different two-neutron decay modes.

V. DISCUSSION

We can compare the present results with those of earlier experiments, as well as with different calculations of the structure of the ^{5}H system. Many calculations suggest that in addition to the ground state, broader resonances corresponding to $3/2^+$ and $5/2^+$ excited states may be present. We have investigated the likelihood of observing excited states of ^{5}H in the $(d,^3\mathrm{He})$ reaction by calculating the spectroscopic overlaps between ^{6}He and different $^5\mathrm{H}(J^\pi)$ configurations using both shell-model, and *ab initio* calculations with the variational Monte Carlo (VMC) and Green's function Monte Carlo (GFMC) techniques [53,54]. The shell-model calculations used the WBT interaction [55] and were performed using the code NUSHELLX [56]. Table III lists the results. Both calculations indicate that the *sd*-shell neutron occupation in ^{6}He needed to reach the $3/2^+$ or $5/2^+$ states in ^{5}H is negligible. For the shell model, the non-p-shell neutron occupation is vanishingly small as are the corresponding spectroscopic factors for $3/2^+$ or $5/2^+$ states. For the more realistic VMC/GFMC calculations, the ground-state spectroscopic factor exceeds those of the excited states by factors of 50 to 100, indicating that any contribution to the $(d,^3\mathrm{He})$ yield from such excited states is insignificant. This observation pertains also to ^{5}H produced from other proton-removal reactions from ^{6}He, such as $^6\mathrm{He}(p,2p)^5\mathrm{H}$. These results justify the omission of higher excited states in ^{5}H when considering data from the $^6\mathrm{He}(d,^3\mathrm{He})^5\mathrm{H}$ reaction.

Prior studies of this reaction, conducted at lower bombarding energies, suggested a lower resonance energy and smaller laboratory width for the ^{5}H ground state than in the present work, more closely in line with the early measurements of Young *et al.* [17]. It is possible that some previous data, when compared to lineshapes appropriately modified by the DWBA suppression of the reaction yield at higher energies,

TABLE III. Spectroscopic overlaps for $^6\mathrm{He}_{\mathrm{g.s.}} \rightarrow {}^5\mathrm{H}(J^\pi) + p$.

Method	$S(1/2^+)$	$S(3/2^+)$	$S(5/2^+)$
VMC/GFMC	1.18	0.0226	0.0172
Shell model	1.992	≈0	≈0

may be consistent with the present results. Although the reaction employed by Young *et al.* was different from that studied in the present measurement, that measurement was done at such a low bombarding energy that the maximum attainable ^{5}H energy was only 2.4 MeV above the $^3\mathrm{H}+2n$ threshold. This low bombarding energy made it impossible for that experiment to be sensitive to broader structures or higher excitation energies in ^{5}H, and likely affected the observed peak energy and width of the structure in the excitation-energy or missing-mass spectra. The cutoff of the proton-energy spectra at low proton energy/larger missing mass in Ref. [17] reflects that effect. Such limitations do not apply to later $^3\mathrm{H}(t,p)^5\mathrm{H}$ results obtained at a much higher bombarding energy, however as those authors comment that the (t,p) reaction may not be optimal for isolating the ^{5}H ground state and it is unclear how the data from the $(d,^3\mathrm{He})$ and (t,p) reactions should be compared. After initial reports of a very narrow ground state from $^3\mathrm{H}(t,p)^5\mathrm{H}$, it was suggested [21,22] that very narrow resolution-limited features in the (t,p) missing-mass spectrum may in fact reflect interference phenomena between different states in ^{5}H.

We also note that the measurement of $^6\mathrm{He}(p,2p)^5\mathrm{H}$ described in Ref. [18] was performed at $36A$ MeV. With a Q value of approximately -20 MeV depending on the mass of ^{5}H, the maximum excitation energy attainable in ^{5}H was near 8 to 10 MeV, in agreement with the acceptance cutoff of that experiment. It is possible that yield at higher ^{5}H excitation energies was not observed in that measurement due to this kinematic cutoff, perhaps also limiting the possible range of energy and width for the ^{5}H ground state.

We have already discussed the influence of momentum matching on possible ^{5}H lineshapes from $(d,^3\mathrm{He})$; as discussed the effect is more significant at lower bombarding energies. While it is difficult to compare the results of the previously published $(d,^3\mathrm{He})$ data [27] and the present results due to uncertainties about the properties of the experimental setup and the influences of the nuclear reaction, it seems possible that the published data could be in at least reasonable agreement with the current data. One very interesting comparison can be made between the proton-knockout data of Meister *et al.* [24] and the present results. As the energies employed in the knockout experiment were very high, it is likely that the ^{5}H profile from that experiment was unaffected by energy-conservation considerations. The spectrum from [24] actually agrees well with the intrinsic lineshape that is used to produce the best fit to our data. Figure 8 shows (a) the present data with best-fit Monte Carlo histogram, and (b) the data of Ref. [24] plotted with the intrinsic line shape that produces the best-fit experimental spectrum for the present data. The resolution from the knockout measurement varied from 150 keV at low nn relative energies to 800 keV at $E(^5\mathrm{H})=8$ MeV, and has a small additional affect on this comparison. Over the range covered the agreement between the previous data and the curve is quite good.

In comparison to published theoretical results, the present results are in better agreement with the calculations that predict a broad ^{5}H ground state, including those of [7,23,32]. The predicted energies from these calculations are also closer to the present resonance energy. We draw particular attention

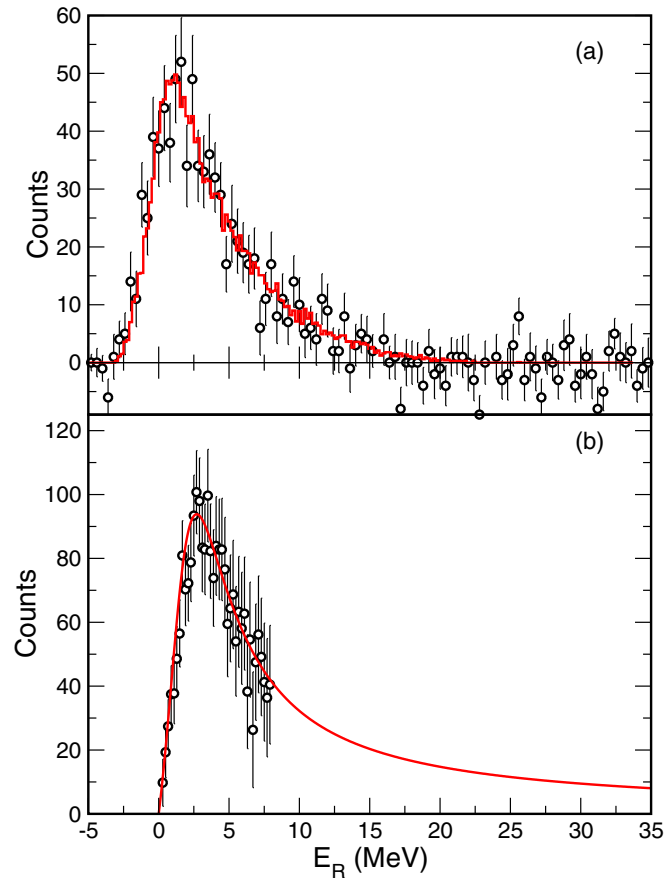

FIG. 8. (a) Current data (points) and experimental best-fit lineshape (histogram); (b) ^{5}H spectrum from $^6\mathrm{He}+{}^{12}\mathrm{C}\rightarrow{}^5\mathrm{H}+X$, data from Ref. [24] (points); best fit "intrinsic" profile from the present results (curve).

to the results presented in [7], where the "Model With Source" (MWS) spectrum obtained with a "normal-sized" source is very close to the intrinsic lineshape that describes the present data. In those calculations, the resonance shape depends on the method of formation (for example, proton removal from ^{6}He) and in turn the effective size of the system. Furthermore, due to the very unbound nature of the system, multi-channel couplings are responsible for additional binding energy. That calculation suggests that two-neutron correlations arising from the initial state in ^{6}He should persist in ^{5}H following proton removal from ^{6}He. While the present experiment does not possess the sensitivity necessary to study such correlations in detail, those ideas strongly motivate additional measurements of two-neutron correlations from ^{5}H decay after formation by proton removal from ^{6}He. The notion that observable properties of the ^{5}H system such as the peak energy and width will depend on the formation mechanism raises important theoretical issues regarding the fundamental nature of such broad resonances that merit further theoretical and experimental study.

With the calculations of Gal and Millener [38], the present mass of ^{5}H may also make it less likely that ${}^6_\Lambda\mathrm{H}$ forms a particle-stable bound state. In Ref. [38], the binding energy of

${}^{6}_{\Lambda}$H is given by $B_{2n}({}^{6}_{\Lambda}\mathrm{H}) = B_{2n}({}^{5}\mathrm{H}) + [B_{\Lambda}({}^{6}_{\Lambda}\mathrm{H}) - B_{\Lambda}({}^{4}_{\Lambda}\mathrm{H})]$. With the current value of $B_{2n}({}^{5}\mathrm{H}) = -2.4$ MeV and the value of $B_{\Lambda}({}^{6}_{\Lambda}\mathrm{H}) - B_{\Lambda}({}^{4}_{\Lambda}\mathrm{H}) = 2.24$ MeV, ${}^{6}_{\Lambda}$H becomes unbound with respect to two-neutron emission. Very similar results are obtained by Himaya *et al.* [39]. Finally, the large width of ^{5}H also suggests that ^{7}H, which should be even broader, will be difficult to observe. Some rough estimates of the ^{7}H width [16] suggest that with the current value of the ${}^{5}\mathrm{H} \rightarrow {}^{3}\mathrm{H} + 2n$ separation energy, the ^{7}H separation energy should be between 4–5 MeV and the width loosely constrained, but possibly as great as 10 MeV or more.

VI. SUMMARY AND CONCLUSIONS

We have performed a new measurement of the ^{6}He$(d,{}^{3}$He$){}^{5}$H reaction at $E({}^{6}\mathrm{He}) = 55A$ MeV. Our data are consistent with a resonance with a laboratory energy 2.4 ± 0.3 MeV above the ${}^{3}\mathrm{H} + 2n$ threshold, and laboratory width of 4.8 ± 0.4 MeV FWHM. When the effects of the suppression of the yield at higher energy due to momentum-matching effects are considered, the "intrinsic" properties of the ^{5}H ground state which would be compared to theoretical predictions are $E_R = 2.4 \pm 0.3$ MeV and $\Gamma = 5.3 \pm 0.4$ MeV. A simultaneous measurement of the ^{5}He ground state with the previously unreported ^{6}He$(d,t){}^{5}$He reaction provides supporting evidence that the present experimental results are reliable.

These values agree with those obtained from some previous measurements of ^{5}H, but conflict with others, in particular previous work using the ^{6}He$(d,{}^{3}$He$){}^{5}$H reaction. Some previous data, when compared to resonances shapes appropriately modified to reflect the dependence of the reaction cross section on Q value and excitation energy, may actually agree better with the current results. The present width continues to conflict with claims of a very narrow ^{5}H ground state. In comparison to theoretical predictions, the current results are most consistent with the calculations presented in [7] and [23]. These new data can provide further guidance for theoretical studies of ^{5}H in particular, as well as for the more general problem of diffuse neutron-rich systems, and suggest that more detailed experiments where neutrons are detected following the population of ^{5}H with the $(d,{}^{3}$He$)$ reaction would be interesting to study to search for pronounced dineutron correlations in the ^{5}H ground state.

ACKNOWLEDGMENTS

The authors wish to thank the staff of the NSCL for their support and for steady and reliable beam delivery throughout the experiment. We also thank J. P. Greene of Argonne National Laboratory for preparation of the targets. This material is based upon work supported by the U. S. Department of Energy, Office of Science, Office of Nuclear Physics, under Awards No. DE-FG02-04ER41320, No. DE-SC0014552, No. DE-FG02-87ER40316, and No. DE-AC02-06CH11357, and the U. S. National Science Foundation under Grants No. PHY-1068192 and No. PHY-1102511.

[1] A. Spyrou, Z. Kohley, T. Baumann, D. Bazin, B. A. Brown, G. Christian, P. A. DeYoung, J. E. Finck, N. Frank, E. Lunderberg, S. Mosby, W. A. Peters, A. Schiller, J. K. Smith, J. Snyder, M. J. Strongman, M. Thoennessen, and A. Volya, Phys. Rev. Lett. **108**, 102501 (2012).

[2] F. M. Marqués, N. A. Orr, N. L. Achouri, F. Delaunay, and J. Gibelin, Phys. Rev. Lett. **109**, 239201 (2012).

[3] A. Spyrou, Z. Kohley, T. Baumann, D. Bazin, B. A. Brown, G. Christian, P. A. DeYoung, J. E. Finck, N. Frank, E. Lunderberg, S. Mosby, W. A. Peters, A. Schiller, J. K. Smith, J. Snyder, M. J. Strongman, M. Thoennessen, and A. Volya, Phys. Rev. Lett. **109**, 239202 (2012).

[4] F. M. Marqués, M. Labiche, N. A. Orr, J. C. Angélique, L. Axelsson, B. Benoit, U. C. Bergmann, M. J. G. Borge, W. N. Catford, S. P. G. Chappell, N. M. Clarke *et al.*, Phys. Rev. C **65**, 044006 (2002).

[5] K. Kisamori, S. Shimoura, H. Miya, S. Michimasa, S. Ota, M. Assie, H. Baba, T. Baba, D. Beaume, M. Dozono *et al.*, Phys. Rev. Lett. **116**, 052501 (2016).

[6] S. C. Pieper, Phys. Rev. Lett. **90**, 252501 (2003).

[7] L. V. Grigorenko, N. K. Timofeyuk, and M. V. Zhukov, Eur. Phys. J. A **19**, 187 (2004).

[8] A. M. Shirokov, G. Papadimitriou, A. I. Mazur, I. A. Mazur, R. Roth, and J. P. Vary, Phys. Rev. Lett. **117**, 182502 (2016).

[9] B. M. K. Nefkens, Phys. Rev. Lett. **10**, 55 (1963).

[10] E. G. Adelberger, A. B. McDonald, T. A. Tombrello, F. S. Dietrich, and A. V. Nero, Phys. Lett. B **25**, 595 (1967).

[11] N. E. Booth, A. Beretvas, R. E. P. Davis, C. Dolnick, R. E. Hill, M. Raymond, and D. Sherden, Nucl. Phys. A **119**, 233 (1968).

[12] A. A. Korsheninnikov, E. Yu. Nikolskii, E. A. Kuzmin, A. Ozawa, K. Morimoto, F. Tokanai, R. Kanungo, I. Tanihata, N. K. Timofeyuk M. S. Golovkov *et al.*, Phys. Rev. Lett. **90**, 082501 (2003).

[13] M. Caamaño, D. Cortina-Gil, W. Mittig, H. Savajols, M. Chartier, C. E. Demonchy, B. Fernandez, M. B. Gomez Hornillos, A. Gillibert, B. Jurado *et al.*, Phys. Rev. Lett. **99**, 062502 (2007).

[14] M. Caamaño, D. Cortina-Gil, W. Mittig, H. Savajols, M. Chartier, C. E. Demonchy, B. Fernandez, M. B. Gomez Hornillos, A. Gillibert, B. Jurado *et al.*, Phys. Rev. C **78**, 044001 (2008).

[15] E. Yu. Nikolskii, A. A. Korsheninnikov, H. Otsu, H. Suzuki, K. Yoneda, H. Baba, K. Yamada, Y. Kondo, N. Aoi, A. S. Denikin *et al.*, Phys. Rev. C **81**, 064606 (2010).

[16] M. S. Golovkov, L. V. Grigorenko, A. S. Fomichev, Yu. Ts. Oganessian, Yu. I. Orlov, A. M. Rodin, S. I. Sidorchuk, R. S. Slepnev, S. V. Stepantsov, G. M. Ter-Akopian, and R. Wolski, Phys. Lett. B **588**, 163 (2004).

[17] P. G. Young, Richard H. Stokes, and Gerald G. Ohlsen, Phys. Rev. **173**, 949 (1968).

[18] A. A. Korsheninnikov, M. S. Golovkov, I. Tanihata, A. M. Rodin, A. S. Fomichev, S. I. Sidorchuk, S. V. Stepantsov, M. L. Chelnokov, V. A. Gorshkov, D. D. Bogdanov, R. Wolski, G. M. Ter-Akopian *et al.*, Phys. Rev. Lett. **87**, 092501 (2001).

[19] M. S. Golovkov, Yu. Ts. Oganessian, D. D. Bogdanov, A. S. Fomichev, A. M. Rodin, S. I. Sidorchuk, R. S. Slepnev, S. V. Stepantsov, G. M. Ter-Akopian, R. Wolski *et al.*, Phys. Lett. B **566**, 70 (2003).
[20] F. C. Barker, Phys. Rev. C **68**, 054602 (2003).
[21] M. S. Golovkov, L. V. Grigorenko, A. S. Fomichev, S. A. Krupko, Yu. Ts. Oganessian, A. M. Rodin, S. I. Sidorchuk, R. S. Slepnev, S. V. Stepantsov, G. M. Ter-Akopian *et al.*, Phys. Rev. Lett. **93**, 262501 (2004).
[22] M. S. Golovkov, L. V. Grigorenko, A. S. Fomichev, S. A. Krupko, Yu. Ts. Oganessian, A. M. Rodin, S. I. Sidorchuk, R. S. Slepnev, S. V. Stepantsov, G. M. Ter-Akopian *et al.*, Phys. Rev. C **72**, 064612 (2005).
[23] N. B. Shul'gina, B. V. Danilin, L. V. Grigorenko, M. V. Zhukov, and J. M. Bang, Phys. Rev. C **62**, 014312 (2000).
[24] M. Meister, L. V. Chulkov, H. Simon, T. Aumann, M. J. G. Borge, Th. W. Elze, H. Emling, H. Geissel, M. Hellstrom, B. Jonson *et al.*, Phys. Rev. Lett. **91**, 162504 (2003).
[25] S. I. Sidorchuk, D. D. Bogdanov, A. S. Fomichev, M. S. Golovkov, Yu. Ts. Oganessian, A. M. Rodin, R. S. Slepnev, S. V. Stepantsov, G. M. Ter-Akopian, R. Wolski *et al.*, Nucl. Phys. A **719**, C229 (2003).
[26] S. V. Stepantsov, M. S. Golovkov, A. S. Fomichev, A. M. Rodin, S. I. Sidorchuk, R. S. Slepnev, G. M. Ter-Akopian, M. L. Chelnokov, V. A. Gorshkov, Yu. Ts. Oganessian *et al.*, Nucl. Phys. A **738**, 436 (2004).
[27] G. M. Ter-Akopian, A. S. Fomichev, M. S. Golovkov, L. V. Grigorenko, S. A. Krupko, Yu. Ts. Oganessian, A. M. Rodin, S. I. Sidorchuk, R. S. Slepnev, S. V. Stepantsov *et al.*, Eur. Phys. J. A **25**, 315 (2005).
[28] Yu. B. Gurov, M. N. Behr, D. V. Aleshkin, B. A. Chernyshev, S. V. Lapushkin, P. V. Morokhov, V. A. Pechkurov, N. O. Poroshin, V. G. Sandukovsky, and M. V. Telkushev, Eur. Phys. J. A **24**, 231 (2005).
[29] Yu. B. Gurov, S. V. Lapushkin, B. A. Cheryshev, and V. G. Sandukovsky, Phys. Part. Nucl. **40**, 558 (2009).
[30] L. V. Grigorenko, Eur. Phys. J. A **20**, 419 (2004).
[31] A. V. Nesterov, F. Arickx, J. Broeckhove, and V. S. Vasilevsky, Phys. Part. Nucl. **41**, 716 (2010).
[32] P. Descouvemont and A. Kharbach, Phys. Rev. C **63**, 027001 (2001).
[33] K. Arai, Phys. Rev. C **68**, 034303 (2003).
[34] A. Adachour and P. Descouvemont, Nucl. Phys. A **813**, 252 (2008).
[35] J. Broeckhove, F. Arickx, P. Hellinckx, V. S. Vasilevsky, and A. V. Nesterov, J. Phys. G **34**, 1955 (2007).
[36] R. de Diego, E. Garrido, D. V. Fedorov, and A. S. Jensen, Nucl. Phys. A **786**, 71 (2007).
[37] M. Agnello, M. Benussi, M. Bertani, H. C. Bhang, G. Bonomi, E. Botta, M. Bregant, T. Bressani, S. Bufalino, L. Busso *et al.*, Phys. Rev. Lett. **108**, 042501 (2012).
[38] A. Gal and D. J. Millener, Phys. Lett. B **725**, 445 (2013).
[39] E. Hiyama, S. Ohnishi, M. Kamimura, and Y. Yamamoto, Nucl. Phys. A **908**, 29 (2013).
[40] D. R. Tilley, C. M. Cheves, J. L. Godwin, G. M. Hale, H. M. Hofmann, J. H. Kelley, C. G. Sheu, and H. R. Weller, Nucl. Phys. A **708**, 3 (2002).
[41] M. S. Wallace, M. A. Famiano, M.-J. van Goethem, A. M. Rogers, W. G. Lynch, J. Clifford, F. Delaunay, J. Lee, S. Labostov, M. Mocko *et al.*, Nucl. Instrum. Methods Phys. Res. A **583**, 302 (2007).
[42] R. J. Charity, J. M. Elson, J. Manfredi, R. Shane, L. G. Sobotka, B. A. Brown, Z. Chajecki, D. Coupland, H. Iwasaki, M. Kilburn *et al.*, Phys. Rev. C **84**, 014320 (2011).
[43] G. F. Bertsch, K. Hencken, and H. Esbensen, Phys. Rev. C **57**, 1366 (1998).
[44] D. E. Gonzalez Trotter *et al.*, Phys. Rev. C **73**, 034001 (2006).
[45] C. Bertulani, L. Canto, and M. Hussein, Phys. Rep. **226**, 281 (1993).
[46] J. F. Ziegler, J. P. Biersack, and U. Littmark, *The Stopping and Range of Ions in Matter* (Pergamon, New York, 1985).
[47] J. F. Ziegler, Nucl. Instrum. Methods Phys. Res. B **219-220**, 1027 (2004).
[48] O. B. Tarasov and D. Bazin, Nucl. Instrum. Methods Phys. Res. B **266**, 4657 (2008).
[49] A. M. Lane and R. G. Thomas, Rev. Mod. Phys. **30**, 257 (1958).
[50] M. H. Mcfarlane and S. C. Pieper, Argonne National Laboratory Report No. ANL-76-11, Rev. 1, 1978 (unpublished).
[51] Haixia An and Chonghai Cai, Phys. Rev. C **73**, 054605 (2006).
[52] D. Y. Pang, P. Roussel-Chomaz, H. Savajols, R. L. Varner, and R. Wolski, Phys. Rev. C **79**, 024615 (2009).
[53] I. Brida, Steven C. Pieper, and R. B. Wiringa, Phys. Rev. C **84**, 024319 (2011).
[54] B. S. Pudliner, V. R. Pandharipande, J. Carlson, Steven C. Pieper, and R. B. Wiringa, Phys. Rev. C **56**, 1720 (1997).
[55] E. K. Warburton and B. A. Brown, Phys. Rev. C **46**, 923 (1992).
[56] B. A. Brown and W. D. M. Rae, Nucl. Data Sheets **120**, 115 (2014).